

Contents lists available at ScienceDirect

Journal of the Mechanics and Physics of Solids

journal homepage: www.elsevier.com/locate/jmps





The role of adhesion on soft lubrication: A new theory

Chung-Yuen Hui a,b,*, Xuemei Xiao c, Hao Dong d, Anand Jagota d,e

- a Sibley School of Mechanical and Aerospace Engineering, Field of Theoretical and Applied Mechanics, Cornell University, Ithaca, NY 14853, USA
- ^b Global Station for Soft Matter, GI-CoRE, Hokkaido University, Sapporo 001-0021, Japan
- ^c Sibley School of Mechanical and Aerospace Engineering, Field of Mechanical Engineering, Cornell University, Ithaca, NY 14853, USA
- ^d Department of Chemical and Biomolecular Engineering, Lehigh University, Bethlehem, PA 18015, USA
- ^e Department of Bioengineering, Lehigh University, Bethlehem, PA 18015, USA

ARTICLE INFO

Keywords: Soft lubrication Instability Adhesion Mixed lubrication

ABSTRACT

Recent experiments reveal that adhesive interactions can play a key role in causing surface instability in soft lubrication. Instances of instability include fluid entrapment in isolated pockets upon a soft sphere's normal contact with a hard substrate and surface wrinkling of a soft substrate as a hard sphere slides across it. These phenomena underscore a substantial distinction between hard and soft lubrication. They are of paramount importance from a fundamental standpoint, providing an entirely new explanation for the transition mechanism from elasto-hydrodynamic to the mixed lubrication regimes. Here, we introduce a new theory to elucidate these observations. Our theory modifies the Reynolds elasto-hydrodynamic equation by incorporating adhesive interaction across the fluid layer, investigating the interplay between adhesion, fluid flow and elastic instability. Our analysis proposes the addition of a new dimensionless parameter in lubrication theory, that compares the stiffness of the adhesive interaction to that of the substrate. When this parameter exceeds unity, the soft solid surface exhibits instability to small perturbations in its shape. In mathematical terms, the Reynolds equation undergoes a transition from a nonlinear diffusion equation to a nonlinear wave equation at this critical point. Post-transition, the diffusivity of the nonlinear diffusion equation turns negative, rendering the problem illposed. We investigate the transition using the method of characteristics and present an exact analytic solution. This solution offers insights into the occurrence of a vanishing liquid film thickness at specific locations, resulting in dry contact—initiating transition to mixed lubrication.

1. Introduction

The study of lubricated contact between hard or stiff solids has been well-established, with mathematical representation through the Reynolds lubrication equation (Cameron, 1971; Reynolds, 1997; Dowson and Higginson, 2014). However, recent interest in the application of soft materials to mechanical (Roberts, 1971; Persson, 2001; Persson et al., 2005; Gervais et al., 2006; Saintyves et al., 2016; Strobel et al., 2012) and biological (Huber et al., 2005; Persson, 2007; Ma et al., 2015; Jahn et al., 2016; Lee et al., 2023) systems has highlighted the challenge of lubricated contact between a soft and a hard solid. In contrast to lubricated contact between stiff solids, this scenario involves intricate interplay among the flow mechanics of the confined fluid, properties of the lubricant and substrate deformation. Many applications involve two distinct contact modes: the first is normal contact (Roberts, 1971; Hou et al.,

E-mail address: ch45@cornell.edu (C.-Y. Hui).

Corresponding author.

1992; Persson et al., 2005; Balmforth et al., 2010; Leroy et al., 2012; Kaveh et al., 2014; Wang et al., 2015, 2017; Karan et al., 2020, 2021; Sun et al., 2021; Liu et al., 2022; Bureau et al., 2023; Jha et al., 2023), where a smooth hard/soft indenter is brought vertically into contact with a lubricated soft/hard elastic substrate, and the second is sliding contact (Persson, 2001; Martin et al., 2002; Skotheim and Mahadevan, 2004; de Vicente et al., 2005; Persson et al., 2005; Persson and Scaraggi, 2009; Myant et al., 2010; Strobel et al., 2012; Ma et al., 2015; Sadowski and Stupkiewicz, 2019; Wu et al., 2020; Hui et al., 2021; Essink et al., 2021; Moyle et al., 2021; Wu et al., 2021, 2023; Dong et al., 2023), where the soft/hard indenter slides across the lubricated surface of a hard/soft substrate. Lubricated sliding generally involves three regimes: boundary (B), mixed (ML), and elasto-hydrodynamic (EHL). In the B regime, the liquid between contact surface pairs is completely expelled; friction response is similar to dry contact (Persson and Scaraggi, 2009; Strobel et al., 2012; Jahn et al., 2016). In contrast, in the EHL regime, a continuous fluid film is present between contact pairs (de Vicente et al., 2005; Dowson and Higginson, 2014; Wang et al., 2015; Sadowski and Stupkiewicz, 2019; Hui et al., 2021; Karan et al., 2021; Moyle et al., 2021; Dong et al., 2023; Jha et al., 2023; Wu et al., 2023). Finally, in the mixed (ML) regime, this continuous film breaks down partially (Spikes, 1997; Ta et al., 2016; Sadowski and Stupkiewicz, 2019; Moyle et al., 2021).

In contrast to the mixed (ML) regime, the theory for the EHL regime is far more comprehensively developed. Consequently, it has been the subject of extensive research, with various factors, including the hydrophilicity of contact pairs (Persson and Scaraggi, 2009; Sun et al., 2021), lubricant types (de Vicente et al., 2005; Strobel et al., 2012; Sadowski and Stupkiewicz, 2019; Dong et al., 2023), surface patterns (Persson, 2001; Sadowski and Stupkiewicz, 2019; Moyle et al., 2021), substrate stiffness (Myant et al., 2010; Kaveh et al., 2014; Dong et al., 2023), sliding velocity (de Vicente et al., 2005; Sadowski and Stupkiewicz, 2019; Dong et al., 2023), viscoelastic effects (Myant et al., 2010; Hui et al., 2021; Wu et al., 2021), and normal loading (Myant et al., 2010; Sadowski and Stupkiewicz, 2019; Karan et al., 2021), considered by numerous researchers. A useful finding, resulting from the appropriate normalization of coupled Reynolds and Hertzian contact equations, indicates that the system response in EHL is governed by a single dimensionless parameter (β) (Snoeijer et al., 2013; Wu et al., 2020), consistent with experimental data (Wu et al., 2020; Bertin et al., 2022). Changes in normal load, sliding velocity, and lubricant viscosity shift the system from EHL to ML, where a discontinuous fluid film persists, and solid–solid contact begins to emerge (Spikes, 1997; Persson and Scaraggi, 2009; Ta et al., 2016; Moyle et al., 2021; Dong et al., 2023).

The transition from EHL to ML poses a fundamental challenge in lubrication theory and has garnered significant attention. While the conventional view relies on a dimensionless number Λ , representing the ratio of film thickness to root-mean-square (RMS) surface roughness, as the criterion for the EHL-ML transition (Spikes, 1997; Bongaerts et al., 2007; Sadowski and Stupkiewicz, 2019), recent findings from our group challenge this perspective, especially in the context of soft lubricated contact (Dong et al., 2023). Specifically, although Λ roughly in the \sim 1–10 range (Spikes, 1997; Bongaerts et al., 2007) is widely accepted as indicative of the EHL-ML transition, our recent experiments reveal that in soft lubricated sliding, the EHL-ML transition can occur for lubricant film thickness orders of magnitude larger than the RMS roughness. This indicates that using Λ as the sole criterion for the EHL-ML transition is inappropriate for soft solids. In our experiments, we observed surface instabilities in the form of wrinkles and fluid trapping between wrinkles. These results align with the known highly nonlinear elasticity of soft materials under dry contact conditions, where experimental and theoretical studies have demonstrated the occurrence of surface folding (van Limbeek et al., 2021), buckling (Song et al., 2008), and creasing (Hong et al., 2009; Glover et al., 2023) under compression and shear. These instabilities likely contribute to the EHL-ML transition by inducing random contact of the solid surfaces. However, there is currently no model that connects these surface instabilities to the EHL-ML transition.

Presumably similar surface instability can also occur under normal lubricated contact. If these instabilities exist, fluid could become trapped between wrinkles, resulting in a significant increase in the volume of fluid trapped underneath the indenter during a relaxation test. In such a test, the indenter is rapidly brought into contact with the substrate and then held fixed. During this period, fluid continuously drains from the contact region, causing the volume of fluid in this region to decrease over time (Liu et al., 2022). The presence of surface instabilities, like wrinkles, can dramatically influence the volume of trapped fluid and rate of water evaluation from the contact region.

This phenomenon was recently observed in the experiments of Sun et al. (2021), where they indented a soft polydimethylsiloxane (PDMS) sphere on a glass substrate in a chamber surrounded by water. During the relaxation period with fixed indenter displacement, they found that the rate of water expulsion from the contact region is three orders of magnitude lower for hydrophobic-hydrophobic (adhesive) contact compared to hydrophobic-hydrophilic (non-adhesive) contact. Their experiments demonstrated that "adhesive interactions cause instability in valleys and lead to a state of more trapped water and less intimate solid–solid contact". In Fig. 2b of their work, Sun et al. (2021) demonstrated a clear competition between wettability and adhesion in their experiments. When wettability prevails on a surface, contact is non-adhesive, resulting in a high rate of water expulsion. This competition is defined by the work of adhesion when solid 1 and solid 2 are immersed in liquid (L), given by (Eq. (2) in their work):

$$W_{1L2} = W_{1A2} - \gamma_L(\cos\theta_{1L} + \cos\theta_{2L}), \tag{1}$$

where W_{1A2} is the work of adhesion of solid 1 and solid 2 in air (*A*), and γ_L is surface energy of the liquid, and θ_{1L} and θ_{2L} are the equilibrium contact angles of a liquid drop on flat solid surfaces 1 and 2 in air respectively. In their experiments, Sun et al. observed that adhesion dominates when $W_{1L2} > 0$. For the rest of this paper, we assume this condition is met.

Motivated by the results of Sun et al. (2021) and our experiments in sliding (Dong et al., 2023), we hypothesize that adhesion plays a crucial role in the formation of surface instability in lubricated contact. In our supplementary materials, we provide experimental evidence indicating that, under dry conditions, the interaction distance between a glass sphere (approximately 4 mm in diameter) and a smooth PDMS substrate falls within the range of 200 nm. Notably, this distance increases with the compliance of the PDMS substrate.

Further elaboration on these experiments will be presented in the discussion, with detailed experimental procedures available in the Supporting Information (SI).

In this work, we focus on the normal contact mode and modify the Reynolds hydrodynamic equation to incorporate adhesive interactions across the fluid layer. We then apply this new theoretical framework to investigate elastic instability using a simple geometrical model. The paper is organized as follows: In Section 2 we use perturbation theory to demonstrate that adhesion can induce flow and instability on an initial flat substrate, i.e., small perturbations can become unstable and grow. We hypothesize that such unstable growth, by increasing friction due to solid-solid contact, can lead to surface wrinkling. We show that instability occurs when a dimensionless parameter $\alpha \ge 1$. α represents the ratio of adhesion stiffness to the stiffness of elastic substrate. It is defined in Eq. (15) and more description can be found in Section 2.4. Moving to Section 3, we employed a fully nonlinear numerical analysis to study the impact of adhesion on lubricant flow. In the regime of $\alpha < 1$, Reynolds equation is mathematically equivalent to a nonlinear heat diffusion equation with temperature dependent diffusion coefficient. We compare the linearized solution from Section 2 with the numerical solution of the nonlinear equations. We show that the 2nd order nonlinear diffusion equation simplifies into a 1st order nonlinear wave equation at the stability transition where $\alpha = 1$. We examine the physical significance and solution of this 1st order nonlinear partial differential equation (PDE). Finally, we conclude the paper with a discussion and summary in Section 4.

2. Linear stability analysis

We study the impact of adhesion on lubricated normal contact using a simple geometry where an infinitely flat rigid indenter is brought into normal contact with a lubricated flat surface of an elastic foundation. Flow is independent of the out of plane direction. The stiffness of the elastic foundation is denoted by *k*. The geometry is illustrated in Fig. 1.

2.1. A homogeneous solution of the Reynolds equation

As shown in Fig. 1(a), the rigid indenter is pushed downward with a vertical displacement $\Delta(t) < 0$. Since the lateral dimension of the indenter is infinite, symmetry implies that the pressure gradient is zero everywhere, so the fluid velocity gradient is zero everywhere and there is no flow. Thus, the fluid pressure is spatially uniform, say, p. The displacement of the substrate foundation w is independent of position and (negative downward) is the same as $\Delta(t)$. The pressure, according to the foundation model is:

$$p = -k\mathbf{w} = -k\Delta(t). \tag{2}$$

Next, we introduce an attractive force between the surfaces resulting in a normal stress σ_{ad} attracting the rigid indenter downwards (the bottom of substrate is fixed). We assume that this stress depends only on the separation h between the flat indenter and the substrate (or the fluid thickness), i.e.,

$$\sigma_{ad} = f(h),$$
 (3)

where f specifies the adhesive interaction and is a monotonic decreasing function of h. For this case, the fluid film thickness is unchanged by the indentation and is h_I (initial fluid thickness). The pressure and displacement are spatially homogeneous, and the Reynolds equation is satisfied trivially. The normal pressure acting on the substrate is $p - f(h_I)$ and the surface displacement of the substrate is $w = \Delta(t)$.

$$p - f(h_l) = -kw = -k\Delta. \tag{4}$$

Thus, given the indentation $\Delta(t)$ and the separation h, we can find the pressure of the fluid layer. For example, if $\Delta(t) = 0$, then

$$p = f(h_l). ag{5}$$

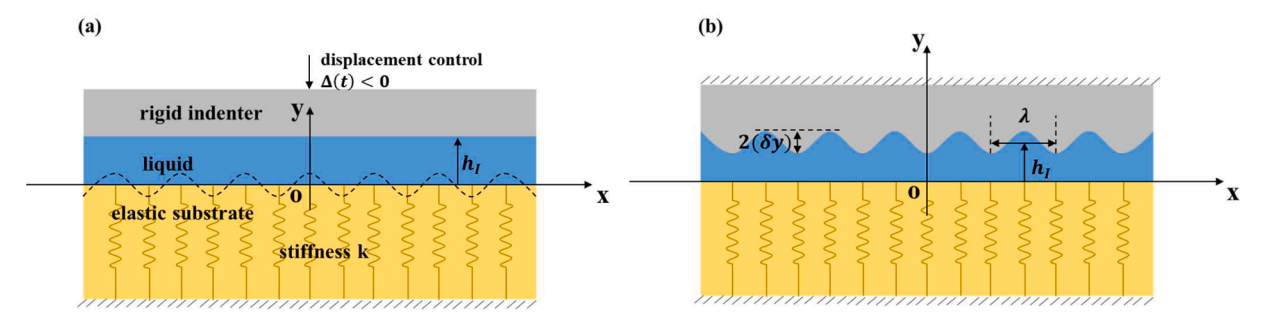


Fig. 1. Schematic diagram of the geometry (not to scale). (a) The three layers (indenter, fluid, and substrate) are infinite in extent in the horizontal (x) and the out of plane directions; the fluid layer has uniform initial thickness h_I . The elastic substrate is modeled as an elastic foundation with stiffness k. The coordinate system (x,y) is placed on the top surface of the undeformed substrate which is y=0 (y>0 upwards). The dash line in black presents the perturbation to the top surface of the substrate used in Sections 2.2 and 2.3. (b) The indenter has cosine undulation with amplitude δy and wavelength λ . The shape undulation here is treated as the defect on the indenter, used in Section 3.

2.2. Stability of homogenous solution

The pressure given by (4) is spatially homogeneous; there is no flow. The question is whether this solution is stable with respect to small perturbations. More specifically, let us allow a small perturbation of the surface of the substrate at t = 0, in the form of

$$y(x, t=0^+) = \delta y \cos(2\pi x/\lambda)$$
, where $\delta y/h_l \ll 1$, (6)

where y=0 corresponds to the position of the unperturbed substrate surface (see Fig. 1(a)). As a result of this perturbation, the pressure field is no longer spatially uniform. Indeed, the initial gap between the surface of the indenter and the substrate is $h(x,t=0^+)=h_I-\delta y\cos(2\pi x/\lambda)$. This means that the fluid film in the perturbed configuration $(t=0^+)$ is narrower in some parts and thicker in others, i.e., the film is thinnest at $x=n\lambda$ (peak) and thickest at $x=\left(n+\frac{1}{2}\right)\lambda$ (valley), where n is an integer. The initial interaction stress is:

$$\sigma_{ad} = f(h_I - \delta y \cos(2\pi x / \lambda)). \tag{7}$$

This stress due to adhesion is highest at the peaks and lowest at the valleys.

2.3. Stability analysis: long wavelength approximation

We use lubrication theory to compute flow. This approximation assumes that the thickness of the fluid layer is much smaller than the wavelength of perturbation, i.e., $h << \lambda$. For this case, h satisfies the Reynolds equation (Cameron, 1971; Reynolds, 1997; Dowson and Higginson, 2014),

$$\frac{\partial h}{\partial t} = \frac{1}{12n} \frac{\partial}{\partial x} \left(h^3 \frac{\partial p}{\partial x} \right),\tag{8}$$

where p is the fluid pressure, η is the fluid dynamic viscosity and h is the thickness of the fluid film and is given by:

$$h(x,t) = h_I - \delta y \cos(2\pi x/\lambda) - (w - \Delta). \tag{9}$$

The vertical displacement of the substrate surface is:

$$w = -(p - \sigma_{ad})/k = [f(h) - p]/k. \tag{10}$$

Impose a perturbation on the homogeneous displacement and pressure field in (4), i.e.,

$$p(x,t) = p_0 + \delta p = f(h_t) - k \Delta(t) + \delta p, \quad w(x,t) = \Delta(t) + \delta w. \tag{11a,b}$$

Using (10),

$$k(\Delta + \delta w) = -p_0 - \delta p + f(h) \Leftrightarrow k \ \delta w = -\delta p + f(h) - f(h_t). \tag{11c}$$

From (11b) and (9),

$$h = h_I - \delta y \cos(2\pi x / \lambda) - \delta w. \tag{11d}$$

For small perturbation,

$$f(h) \approx f(h_I) + (h - h_I) f'(h_I). \tag{12}$$

where f' = df/dh. Substituting (12), (11d) into (11c), we get

$$\delta p = -k \, \delta w + f(h) - f(h_l) \approx -k \, \delta w - [\delta y \cos(2\pi x/\lambda) + \delta w] \, f(h_l). \tag{13}$$

Using (11a), we have $\frac{\partial p}{\partial x} = \frac{\partial \delta p}{\partial x}$, so to leading order, the Reynolds Eq. (8) is:

$$\frac{\partial h}{\partial t} = -\frac{\partial \delta w}{\partial t} \approx \frac{h_i^3}{12\eta} \frac{\partial^2 \delta p}{\partial x^2}.$$
 (14)

Substituting (13) into (14), we obtain

$$\frac{\partial \delta w}{\partial t} - \frac{(1-\alpha)kh_I^3}{12\eta} \frac{\partial^2 \delta w}{\partial x^2} = \frac{\alpha kh_I^3}{12\eta} \delta y \left(\frac{2\pi}{\lambda}\right)^2 \cos(2\pi x/\lambda), \quad \alpha \equiv -f(h_I) / k \ge 0. \tag{15}$$

Since the initial perturbation is periodic, we seek a periodic solution of (15) that satisfies the initial condition $\delta w(t=0)=0$. It is easy to verify this solution is:

$$\delta w = \frac{\alpha \, \delta y}{1 - \alpha} [1 - \exp(bt)] \cos(2\pi x \, / \, \lambda),\tag{16a}$$

where

$$b = -\frac{(1-\alpha)kh_l^3}{12\eta} \left(\frac{2\pi}{\lambda}\right)^2. \tag{16b}$$

Note when b > 0 or a > 1, the solution is unstable since the displacement of the substrate will grow exponentially fast with time.

2.4. Comments

- A special case which contains most of the essential physics is $\Delta=0$, that is, when flow is driven entirely by adhesion. The analysis conducted earlier, specifically in Eq. (15), governing the temporal and spatial evolution of displacement and pressure, unveils that it remains unaffected by Δ . Consequently, we concentrate on this $\Delta=0$ case for the remainder of this paper.
- Eq. (15) can be identified as a linear heat diffusion equation with diffusion coefficient given by $\frac{(1-\alpha)kh_1^3}{12\eta}$. The heat source is given by the RHS of (15). Instability corresponds to a *negative diffusion coefficient* where $\alpha > 1$.
- Stability is controlled by a dimensionless parameter $\alpha \equiv -f'(h_I)/k \geq 0$. The physical interpretation of this parameter is as follows: $f'(h_I)$ represents the slope of adhesive stress versus gap thickness at h_I , serving as the intrinsic stiffness of an adhesive "spring" with negative value, i.e., force increases with decreasing distance. In contrast, the substrate stiffness, k, is positive. Visualize a spring-block system where these springs are connected in series. When $-f'(h_I) > k$ (or when $\alpha > 1$), if the block retracts the attractive force increases more than required to hold the spring in place and we have a mechanically unstable jump into contact.

3. Evolution of interface due to adhesion - nonlinear theory

The above analysis linearizes the nonlinear Reynolds equation. In this section we study the evolution of displacement and pressure by solving the nonlinear Reynolds equation and compare these results with the linearized theory in the previous section. Detailed analysis is carried out in two regimes: $\alpha < 1$, $\alpha = 1$. In the regime of $\alpha > 1$, the numerical scheme is unstable.

First, we modified Reynolds equation for normal contact. Here we consider the case where the rigid plate is fixed (i.e., $\Delta=0$), so the change in liquid film thickness/pressure is driven solely by adhesion. The dependence of stability on applied displacement and machine compliance is provided in Section 3 of the SI. For convenience, we treat the perturbation as a permanent geometric defect as shown in Fig. 1(b), that is, the rigid indenter is not exactly flat, instead, its surface varies sinusoidally with amplitude $\delta y>0$. Specifically, the film thickness is given by:

$$h = h_I - \delta y \cos(2\pi x / \lambda) - w. \tag{17}$$

To simplify the analysis, we assume a piecewise linear adhesion model (Camacho and Ortiz, 1996), i.e.,

$$\sigma_{ad}(h) = \begin{cases} \sigma_0(1-h/d_c) \ 0 < h \le d_c \\ 0 \qquad \qquad h > d_c \end{cases}, \tag{18a,b}$$

where σ_0 , and d_c are material constants. At h=0, there is hard contact. Physically, σ_0 indicates the adhesive strength and d_c is a characteristic distance over which adhesion acts. The quantity $\sigma_0 d_c/2$ (area underneath the σ_{ad} vs h plot) is typically referred to as the work of adhesion in Fracture Mechanics (Maugis, 1992). If we further assume that $h \le d_c$ (this assumption is usually satisfied for sufficiently small h_l), then the fluid pressure p everywhere can be computed using (10), (17), and (18a), with $f(h) = \sigma_0(1 - h/d_c)$. The Reynolds Eq. (8) becomes (by substituting the p in expression of fluid thickness h):

$$\frac{\partial h}{\partial t} = \frac{k}{12\eta} \frac{\partial}{\partial x} \left\{ h^3 \frac{\partial}{\partial x} \left[h - h_l + \delta y \cos\left(\frac{2\pi x}{\lambda}\right) + \frac{\sigma_0}{k} \left(1 - \frac{h}{d_r}\right) \right] \right\}$$

with

$$p = f(h) - kw = \sigma_0 \left(1 - \frac{h}{d_r} \right) + k[h - h_I + \delta y \cos(2\pi x / \lambda)]. \tag{19}$$

We introduce the following normalization to expedite the analysis,

$$X = 2\pi x / \lambda, \ H = h / h_I, \ W = w / h_I, \ T = t \left[\frac{k h_I^3}{12 \eta} \left(\frac{2\pi}{\lambda} \right)^2 \right]. \tag{20a-d}$$

Using these normalizations, (19) can be written as

$$\frac{\partial H}{\partial T} - (1 - \alpha) \frac{\partial}{\partial X} \left(H^3 \frac{\partial H}{\partial X} \right) = -\epsilon \frac{\partial \left(H^3 \sin X \right)}{\partial X},\tag{21a}$$

where

$$\alpha = \sigma_0/(kd_c) > 0, \ 0 < \epsilon \equiv (\delta y)/h_t < 1, \ H = 1 - \epsilon \cos X - W.$$
 (21b-d)

Note that if we interpret H as temperature, then $(1-\alpha)H^3$ can be interpret as a temperature dependent diffusivity which depends on the temperature to the third power. Hence (21a) can be viewed as a nonlinear heat diffusion equation with temperature dependent diffusivity and $S \equiv -\epsilon \frac{\partial (H^3 \sin X)}{\partial X}$ is a temperature dependent heat source. The initial condition (IC) is:

$$H(X, T=0) = 1 - \epsilon \cos X \Leftrightarrow W(X, T=0) = 0. \tag{22a}$$

The solution of (21a) and (22a) is periodic with period 2π , and symmetry dictates that we need only to consider the region $X \in [0, \pi]$ with boundary conditions (BCs):

$$\frac{\partial H}{\partial X}\Big|_{X=0,\pi} = 0.$$
 (22b)

First, consider the trivial case of NO adhesion, $\alpha = 0$, then $H(X, T) = 1 - \epsilon \cos X$ satisfies all the boundary conditions and the PDE (21) exactly. As expected, nothing happens if there is no adhesion.

It can be verified that, as long as $W \ll 1$, the *linearized* solution of (21a) with $\epsilon \ll 1$ subjected to the IC and BCs (22a, 22b) is given by (16a, 16b), which in normalized form, is:

$$W = \frac{\alpha \epsilon}{1 - \alpha} (1 - \exp[-(1 - \alpha)T])\cos X, \ W \ll 1.$$
 (23a)

Eq. (23a) indicates that, as long as $\alpha < 1$, the displacement does not increase exponentially with time. More importantly, for large $(1 - \alpha)T >> 1$, the exponential goes to zero, and

$$W(X, T \to \infty) = \frac{\alpha \epsilon}{1 - \alpha} \cos X. \tag{23b}$$

Since $H = 1 - \epsilon \cos X - W$ (21d), dry contact occurs first at X = 0 when the condition:

$$W(X=0,T)=1-\epsilon \tag{24a}$$

is satisfied. This condition and (23a) predict that, when $1 - \epsilon < \alpha$, dry contact occurs at X = 0 at normalized time T_c given by

$$(1-\alpha)T_c = -\ln\left[1 - \frac{(1-\alpha)(1-\epsilon)}{\alpha\epsilon}\right] \text{ for } 1 - \epsilon \le \alpha$$
 (24b)

Note the special case of $1-\epsilon=\alpha$ predicts dry contact at infinite time. On the other hand, dry contact will not occur if $1-\epsilon>\alpha$. Here we emphasized that the linearized solution given by (23a, 23b) breaks down for finite times before dry contact can occur, since the displacement will no longer be of order ϵ . For small α so that $\epsilon+\alpha\ll 1$, one expects the solution given by (23a) is uniformly valid for all times, since the displacement remains small. In other words, whether dry contact can occur for $\alpha<1$ should be further studied by solving the nonlinear equation, which is done in Section 3.1.

An important observation is that when $\alpha \rightarrow 1$, the linearized displacement solution given by (23a) approaches:

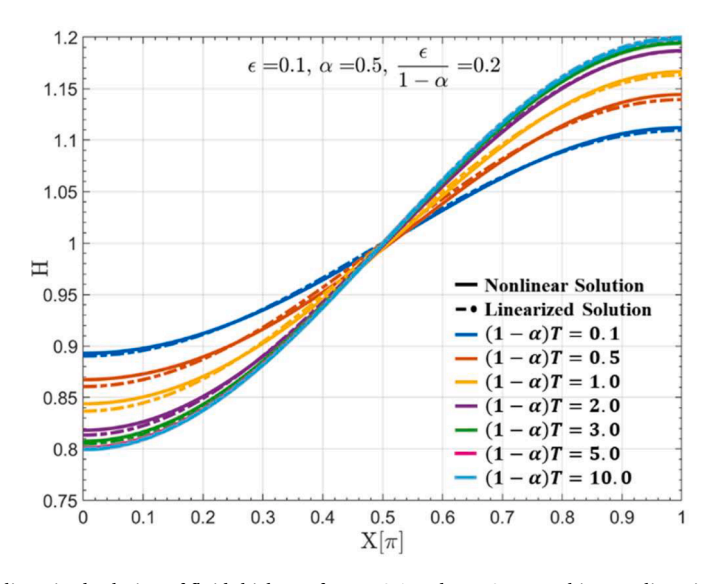


Fig. 2. Nonlinear solution and linearized solution of fluid thickness for e = 0.1 and $\alpha = 0.5$. For this case, linearized solution predicts there would be no dry contact.

$$W = \frac{\alpha \epsilon}{1 - \alpha} (1 - \exp[-(1 - \alpha)T]) \cos X \Rightarrow_{\alpha \to 1} \epsilon T \cos X.$$
 (25)

Thus, the transition to instability at $\alpha=1$ is marked by displacement growing *linearly* with normalized time. Note that the linearized theory predicts that dry contact (i.e., $H=1-\epsilon \cos X-W=1-\epsilon \cos X-\epsilon T\cos X=0$) occurs at X=0 when $T=(1-\epsilon)/\epsilon\approx 1/\epsilon$.

3.1. Numerical solution for $0 < \alpha < 1$

In this regime the surface is stable, but it is still interesting to consider how the surface evolves due to adhesion driven flow. Using a newly developed numerical technique (Liu et al., 2022; Wu et al., 2023), we solved the nonlinear PDE (21) subjected to (22a, 22b) for different values of $\alpha < 1$. Details of implementation are given in the Supporting Information. Comparison of the linearized solution (23a) and the fully nonlinear solution is plotted in Figs. 2-5 for $\epsilon = 0.1$ and $\alpha = 0.5$, 0.8, 0.9 and 0.95 respectively. The figures depict the spatial variation of film thickness H at different times. Since Eq. (23a) indicates that the time dependence is governed by the factor $(1 - \alpha)T$, we vary this parameter in our plots instead of T. These numerical results also allow us to determine elastic foundation displacement fields W at different times, these are given in SI Figures S2-S5. The fluid thickness and displacement fields for $\epsilon = 0.1$ and $\alpha = 0.1$, 0.905, 0.91, 0.92, 0.98 and 0.99 are shown in SI Figures S6-S11 respectively. At $(1-\alpha)T=5$, the fluid thickness and displacement fields with different values of α are shown in SI Figure S12.

Figs. 2-5 demonstrate that the linearized solution agrees well with the nonlinear solution for all $\alpha<1$ for short times, $(1-\alpha)T\ll 1$. For $\alpha\leq 0.8$, the linearized solution accurately predicts the trend, albeit with errors emerging at larger times. It is worth noting that according to the linearized theory, dry contact occurs at X=0 when $1-\epsilon\leq\alpha$. Assuming linear theory is accurate, for $\epsilon=0.1$, dry contact $(H\to 0)$ should occur at sufficiently long times when $\alpha=0.9$ ($\frac{\epsilon}{1-\alpha}=1$). However, the nonlinear solution reveals that although the liquid gap decreases over time, it is not nearly as thin as predicted by the linearized solution. An intriguing observation is that this thin liquid gap extends over a much larger area, while the thinner gap predicted by the linearized solution is more localized at X=0. This trend continues for $1-\epsilon<\alpha$ (or $\epsilon/(1-\alpha)>1$), as illustrated in Fig. 5. Note that for several of the cases, the linearlized solution predicts negative H, which is not permitted physically. In those cases, for the sake of plotting, we assign all negative H values to be zero.

3.2. The transition case $\alpha = 1$

The transitional case holds significance as it allows for exact analysis and illustrates the onset of instability. When instability sets in $\alpha > 1$, the modified Reynolds Eq. (21) becomes numerically unstable, we are not aware of any numerical method to solve this problem. For the transition case $\alpha = 1$, eq. (21a) simplifies to

$$\frac{\partial H}{\partial T} - (1 - \alpha) \frac{\partial}{\partial X} \left(H^3 \frac{\partial H}{\partial X} \right) = -\epsilon \frac{\partial \left(H^3 \sin X \right)}{\partial X} \Rightarrow \frac{\partial H}{\partial T} + 3\epsilon H^2 \sin X \frac{\partial H}{\partial X} = -\epsilon H^3 \cos X. \tag{26}$$

Note the PDE (26) completely changes character when $\alpha = 1$. Instead of a nonlinear diffusion equation ($\alpha < 1$) of 2nd order, it becomes a 1st order hyperbolic equation. This type of equation can be solved using the method of characteristics. The characteristic curves are space curves in the (T, X, H) space. The theory of PDE tells us that these characteristic curves span the solution surface

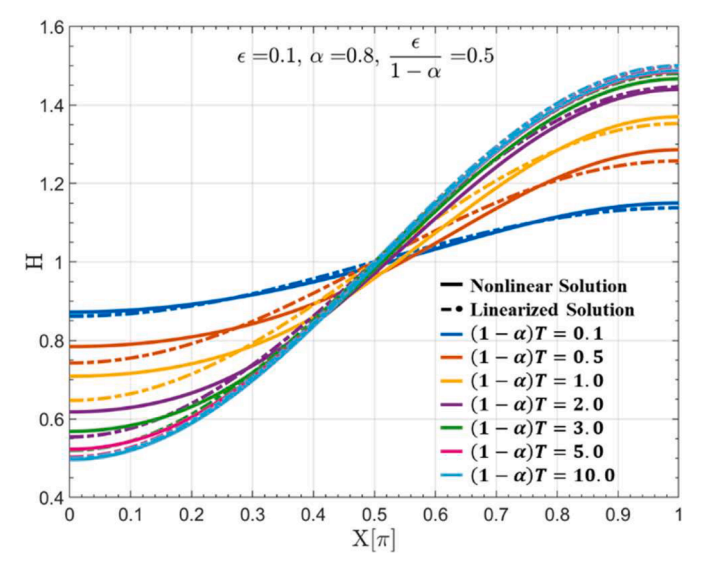


Fig. 3. Nonlinear solution and linearized solution of fluid thickness for $\epsilon = 0.1$ and $\alpha = 0.8$. For this case, linearized solution predicts there would be no dry contact.

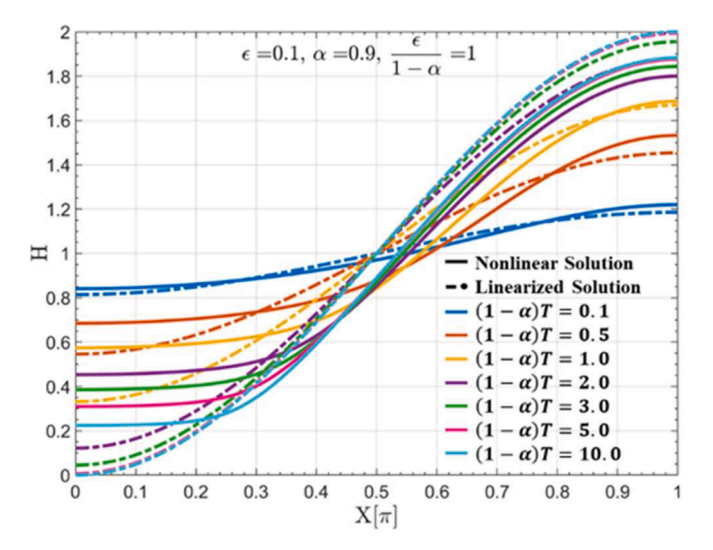


Fig. 4. Nonlinear solution and linearized solution of fluid thickness for $\epsilon = 0.1$ and $\alpha = 0.9$. For this case, linearized solution predicts that dry contact would occur in an infinite time.

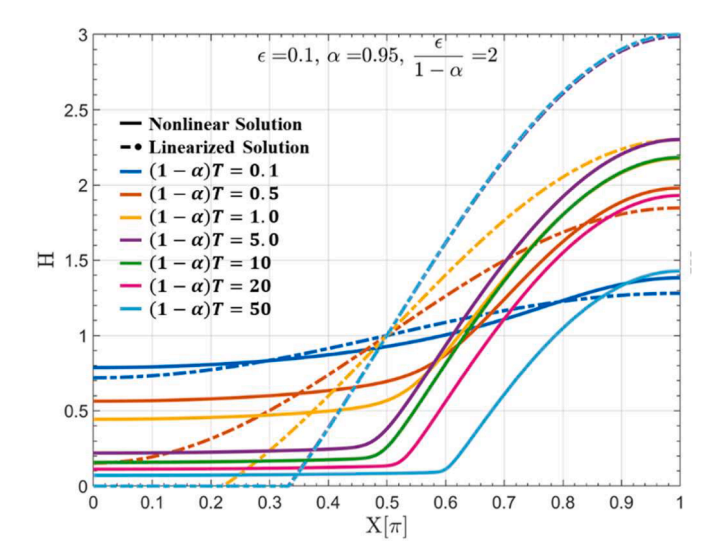


Fig. 5. Nonlinear solution and linearized solution of fluid thickness for $\epsilon = 0.1$ and $\alpha = 0.95$. For this case, linearized solution expects the dry contact would first occur at $(1 - \alpha)T_c = 0.642$. For accuracy, we round up to three decimal places with our numerical time increment as 0.001.

(Carrier and Pearson, 2014). For convenience, we use normalized time *T* to parameterize the characteristic curves, which are solutions of the system of autonomous ordinary differential equations (ODEs) given by:

$$\begin{cases} \frac{dX}{dT} = 3\epsilon H^2 \sin X \\ , \\ \frac{dH}{dT} = -\epsilon H^3 \cos X \end{cases}$$
 (27a,b)

with the initial data

$$H(X, T=0) = 1 - \epsilon \cos X. \tag{27c}$$

For short times, the leading order approximation of (26) is:

$$\frac{\partial H}{\partial T} \approx -\epsilon \frac{\partial \sin X}{\partial X} = -\epsilon \cos X \Rightarrow H = 1 - \epsilon \cos X - \epsilon T \cos X + O(\epsilon^2). \tag{28}$$

Eq. (28) is Eq. (25) for short times.

We integrate (27a, 27b) to determine the evolution of the initial data. Periodicity and symmetry allow us to consider $X \in [0,\pi]$. For example, suppose we want to determine how the film thickness at X = 0 evolves with time, we solve (27a, 27b) subjected to the initial condition:

$$X(T=0) = 0, H(T=0) = 1 - \epsilon.$$
 (29a,b)

It can be easily verified that:

$$X(T \ge 0) = 0, \ H(T) = \left[(1 - \epsilon)^{-2} + 2\epsilon T \right]^{-\frac{1}{2}}$$
 (30a)

satisfies the ODE and the IC. There is also an exact result at $X = \pi$, here the exact solution of (27a, 27b) is:

$$X(T \ge 0) = \pi, \ H(T) = \left[(1 + \epsilon)^{-2} - 2\epsilon T \right]^{-\frac{1}{2}}.$$
 (30b)

These are two important results, as they show exactly how the liquid gap changes with time at the narrowest and widest gap. In dimensional form, these results are:

$$h(x=0,t) = h_I \left[(1-\epsilon)^{-2} + \epsilon \frac{kh_I^3}{6\eta} \left(\frac{2\pi}{\lambda} \right)^2 t \right]^{-\frac{1}{2}},\tag{31a}$$

$$h\left(x = \frac{\lambda}{2}, t\right) = h_I \left[(1 + \epsilon)^{-2} - \epsilon \frac{k h_I^3}{6\eta} \left(\frac{2\pi}{\lambda}\right)^2 t \right]^{-\frac{1}{2}}.$$
 (31b)

Note at $X=\pi$, the gap is infinite as T approaches $1/\left[2\epsilon(1+\epsilon)^2\right]$, presenting an unphysical outcome. This result stems from our calculation assumes that $h \leq d_c$ or $H \leq d_c/h_l$ holds for all X. However, this condition is violated for sufficiently large time when H exceeds d_c/h_l . Therefore, the solution (30b, 31b) is valid for T less than $\left[\left(1+\epsilon\right)^{-2}-\left(h_l/d_c\right)^2\right]/(2\epsilon)$. However, we emphasize that (30a) is valid for all times, which means that, in practice, dry contact will occur at sufficiently long time.

Note that for short times where $2\epsilon T < 1$,

$$H(X=0,T) = \left[(1-\epsilon)^{-2} + 2\epsilon T \right]^{-\frac{1}{2}} \approx 1 - \epsilon - (1-\epsilon)^3 \epsilon T \approx 1 - \epsilon - \epsilon T, \tag{32a}$$

$$H(X = \pi, T) = \left[(1 + \epsilon)^{-2} - 2\epsilon T \right]^{-\frac{1}{2}} \approx 1 + \epsilon + (1 + \epsilon)^3 \epsilon T \approx 1 + \epsilon + \epsilon T.$$
(32b)

We recover the asymptotic solution (28) evaluated at X=0 and π respectively. The time it takes to achieve dry contact depends on the initial amplitude of perturbation, from (30a), T has to be larger than $1/\epsilon$. We next solve (27a, 27b) for $X \in (0, \pi)$. Pick any point $X_1 \in (0, \pi)$, the characteristic curve that intersects this point at T=0 must satisfy, by (27a, 27b),

$$\frac{dH}{dX} = -\frac{H}{3} \frac{\cos X}{\sin X} \Rightarrow H = C_1 (\sin X)^{-\frac{1}{3}},\tag{33}$$

$$\frac{dX}{dT} = 3\epsilon C_1^2 (\sin X)^{1/3} \Rightarrow \int_{X}^{X} \frac{dq}{(\sin q)^{1/3}} = 3\epsilon C_1^2 T. \tag{34}$$

Note we have imposed the condition $X(T=0)=X_1$ in (34). Since the integral in (34) is monotonically increasing, its inverse function must exit, so there exists a function g such that:

$$\int_{X_{-}}^{X} \frac{dq}{\left(\sin q\right)^{1/3}} = 3\epsilon C_1^2 T \Rightarrow X = g\left(3\epsilon C_1^2 T, X_1\right). \tag{35}$$

Finally, C_1 is determined by the initial data and (33), i.e.,

$$1 - \epsilon \cos X_1 = C_1 (\sin X_1)^{-\frac{1}{3}} \Rightarrow C_1 = (1 - \epsilon \cos X_1) (\sin X_1)^{\frac{1}{3}}. \tag{36}$$

Eqs. (33)–(36) completely determine the characteristic curve that passes through the initial curve at $(T=0, X=X_1, H=1-\epsilon\cos X_1)$. Specifically, the characteristic space curve that passes through $(T=0, X=X_1, H=1-\epsilon\cos X_1)$ has coordinates:

$$\left(T = 0, \ X = g\left(3\epsilon C_1^2 T, \ X_1\right), \ H = C_1(\sin X)^{-\frac{1}{3}}\right), \text{ where } C_1 = (1 - \epsilon \cos X_1)(\sin X_1)^{\frac{1}{3}}.$$
(37)

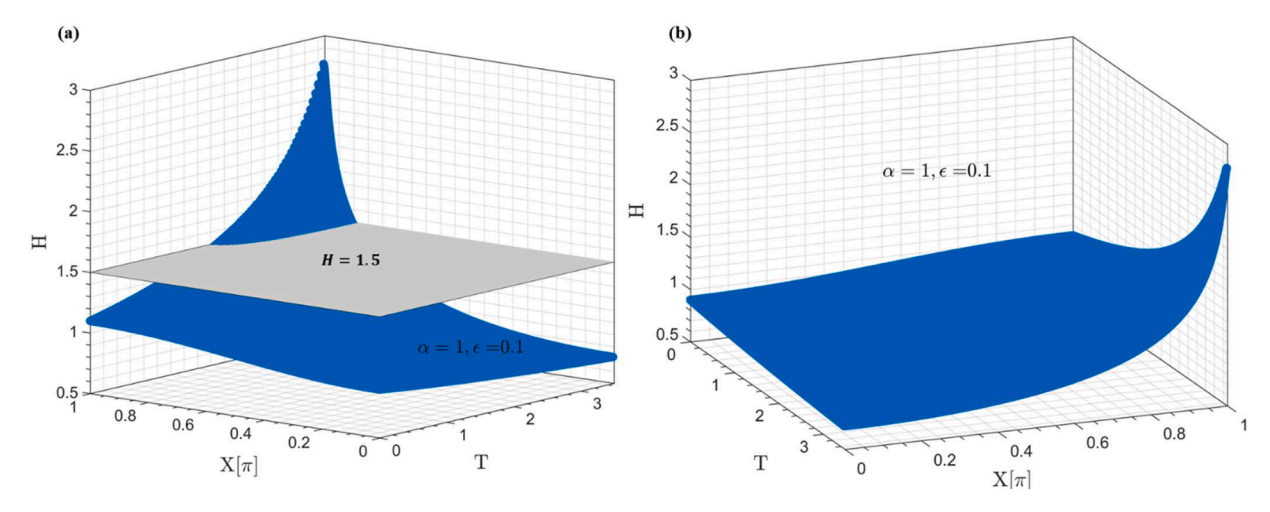


Fig. 6. (X, T, H) solution surface for $\alpha = 1$. In (a), a cut plane in grey color represents the case where $d_c/h_l = 1.5$, serving as an example. Above the cut plane, the solution surface is not valid since (18a) is violated when $H > d_c/h_l$. (b) is a rotated view of (a) to provide a different perspective of the solution surface. If there comes a point in time when the fluid thickness H exceeds d_c/h_l , our solution becomes invalid from that moment onward.

These solutions can also be visualized by examining the phase plane of (27a, 27b). In theory, one can obtain the solution surface by solving the equation:

$$\int_{X_1}^{X} \frac{dq}{(\sin q)^{1/3}} = 3\epsilon (1 - \epsilon \cos X_1)^2 (\sin X_1)^{\frac{2}{3}} T$$
(38)

for X_1 . Denote this solution by $X_1 = \Psi(X, T, \epsilon)$ and substituting this into C_1 in (36) and using (33) gives the equation of the solution surface. In practice, Ψ can be not determined in close form, so this method is not particularly useful. Here we generate the solution surface by computing the characteristic curves by solving (27a, 27b) using many sets of initial data with different $X_1 \in [0, \pi]$. These characteristic curves are then used to span the solution surface which is shown in Fig. 6. For a given time T, we can find the intersection curve H(X,T) of the solution surface and the fixed T surface. The fluid thickness for $\alpha=1$ at different times is plotted in Fig. 7. The corresponding elastic foundation displacement fields are shown in SI Figure S13.

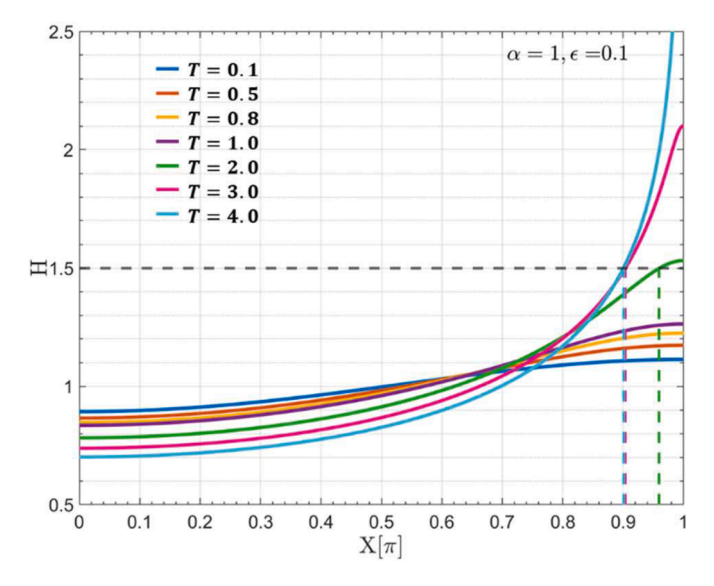


Fig. 7. The fluid thickness H as a function of location X at different time T for $\alpha=1$. Again, we use $d_c/h_l=1.5$ as an illustrative example to demonstrate the valid zone of our solution. The results indicate that for $T=0.1,\ 0.5,\ 0.8,\ 1.0$, the fluid thickness at all X positions satisfies $H< d_c/h_l$, so the solutions are valid. However, for $T=2.0,\ 3.0,\ 4.0$, there are areas where the fluid gap is larger than $d_c/h_l=1.5$. In these regions, our assumption (18a) fails, rendering invalid solutions for such times. The dash lines label the positions where $H(X,T)=d_c/h_l$.

3.3. $\alpha > 1$

As previously mentioned, this scenario corresponds to backward diffusion, where the diffusivity is negative. Even in the case of a linear PDE with a negative constant diffusion coefficient, backward diffusion is recognized as ill-posed, indicating that the solution does not exhibit continuous dependence on the provided data (Zhang and Zhang, 2020). Unfortunately, due to the nonlinearity and unstable nature of (21a), we have not been able to develop a numerical scheme to accurately solve the nonlinear PDE (21) with IC (22a) and BCs (22b).

Herein, we study the outcomes of linear stability analysis and shed light on the anticipated behavior of the nonlinear solution. The linear analysis for this case reveals flow instability. Assuming that W << 1 or H is close to 1, the solution of (21a), (22a, 22b) is given by:

$$H = 1 + \frac{\epsilon}{\alpha - 1} \cos X - \frac{\alpha \epsilon}{\alpha - 1} \cos X \exp[(\alpha - 1)T]. \tag{39}$$

Thus, for $|X| < \pi/2$, H decreases exponentially fast with time. In this region, linearized theory predicts that dry contact is achieved exponentially fast in finite time T_c ,

$$T_c = \frac{1}{\alpha - 1} \ln \left(\frac{1}{\alpha} + \frac{\alpha - 1}{\alpha \epsilon \cos X} \right), \ |X| < \frac{\pi}{2}. \tag{40}$$

However, it is crucial to note that this expression overestimates the contact time. As H decreases, the "diffusion" coefficient (assumed to be $(1-\alpha)H^3$ in perturbation theory) and the "source" term, $-\epsilon \ \partial(H^3 \sin X)/\partial X$, cease to remain constant but decrease rapidly proportional to H^3 . Consequently, the attainment of dry contact is expected to be notably slower than predicted by linear analysis, as exemplified by our results in Fig. 5 (and Figures S7-S11 in SI). In essence, as the liquid gap closes, flow becomes exceedingly sluggish, requiring significantly more time to achieve dry contact. The outcome is the rapid spreading of this thin fluid layer from X=0 to the rest of the region. Hence, linear analysis is expected to provide a lower bound for the time to achieve dry contact.

4. Summary and discussion

Motivated by recent experiments demonstrating the significant role of adhesion in controlling soft contact mechanics under lubricated conditions, we have introduced a new model that integrates adhesive interactions into the standard lubrication equation of Reynolds. Our focus is on examining the impact of adhesion on fluid flow, employing a simple geometry where a thin layer of fluid, initially of constant thickness, is sandwiched between a rigid flat indenter and the surface of an elastic foundation.

We present solutions for flow driven by adhesion and demonstrate that, for a dimensionless parameter α , the homogeneous solution (indicating no flow) becomes unstable, leading to the possibility of dry contact. Mathematically, the modified Reynolds equation transforms from a nonlinear diffusion equation with positive diffusivity to one with negative diffusivity, representing backward diffusion. In the transition case of $\alpha=1$, the Reynolds equation shifts to a first-order nonlinear wave equation. These findings hold significant importance as they provide insights into new phenomena such as fluid trapping under normal contact conditions and surface wrinkling instabilities recently observed in sliding lubricated contact.

For mathematical simplicity, we model the substrate as an elastic foundation. Although it is straightforward to formulate the problem using a finite layer of linear elastic solid, analytic solutions become much more challenging. Nonetheless, we anticipate that a parameter similar to α exists and that there are little qualitative differences in physics. We employ a piecewise linear adhesion model with two parameters, σ_0 and d_c . These parameters can be adjusted to match different surface interactions, such as Van der Waals interactions modified by a thin liquid layer. If necessary, the model can be further modified to represent more accurate interaction between surfaces. In the realm of fracture mechanics and adhesion literature, it is widely accepted that the pivotal parameters in adhesive models are the peak stress and the adhesive energy, the latter being represented by the area under the σ_{ad} versus h curve. The precise shape of the curve holds secondary importance. Therefore, if these two parameters are assumed to be identical, one can anticipate minimal qualitative deviations in the solution behavior, regardless of the specific adhesive model employed. A more complex challenge arises when incorporating curvature into the analysis, as many contact problems involve non-conformal bodies like spheres or cylinders. Despite the formulation remaining the same, the primary obstacle lies in numerically solving highly nonlinear coupled partial differential equations with complicated geometrical boundary conditions. In this work, we study only normal contact. The effect of adhesion on sliding contact will be analyzed in future work.

Finally, we examine the range of adhesive interactions in the soft materials used in our experiments and those of Sun et al. (2021). Here, we discuss results under dry contact conditions which are much easier to observe. In this experiment, a borosilicate glass indenter, 4.06 mm in diameter, approached a PDMS substrate at a velocity of 5×10^{-8} m/s. Using a custom Johnson-Kendall-Roberts (JKR) setup and a high-speed camera, Newton's rings were observed as the indenter moved towards the surface. The sudden jump distance, reflecting the minimum air gap length, was measured before contact. Experiments were conducted on both stiff (with shear modulus G = 1 MPa) and soft (with G = 40 KPa) PDMS substrates. The sudden jump distance for stiff and soft substrate is 195 nm and 250 nm respectively. This result shows that the range of adhesive interactions can be significantly larger than the surface roughness of PDMS substrates (with root-mean-square surface roughness 3.2 nm (Dong et al., 2023)).

CRediT authorship contribution statement

Chung-Yuen Hui: Conceptualization, Formal analysis, Funding acquisition, Investigation, Methodology, Supervision, Writing – original draft, Writing – review & editing. Xuemei Xiao: Formal analysis, Validation, Visualization, Writing – review & editing. Hao Dong: Formal analysis, Writing – review & editing. Anand Jagota: Conceptualization, Funding acquisition, Writing – review & editing.

Declaration of competing interest

The authors declare that they have no known competing financial interests or personal relationships that could have appeared to influence the work reported in this paper.

Data availability

Data will be made available on request.

Acknowledgement

The authors acknowledge the support from the National Science Foundation, CMMI-1854572.

Supplementary materials

Supplementary material associated with this article can be found, in the online version, at doi:10.1016/j.jmps.2024.105720.

References

Balmforth, N.J., Cawthorn, C.J., Craster, R.V., 2010. Contact in a viscous fluid. Part 2. A compressible fluid and an elastic solid. J. Fluid Mech. 646, 339–361. https://doi.org/10.1017/S0022112009993168.

Bertin, V., Amarouchene, Y., Raphaël, E., Salez, T., 2022. Soft-lubrication interactions between a rigid sphere and an elastic wall. J. Fluid Mech. 933, A23. https://doi.org/10.1017/jfm.2021.1063.

Bongaerts, J.H.H., Fourtouni, K., Stokes, J.R., 2007. Soft-tribology: lubrication in a compliant PDMS–PDMS contact. In: Tribol. Int., Tribology at the Interface: Proceedings of the 33rd Leeds-Lyon Symposium on Tribology (Leeds, 2006), 40, pp. 1531–1542. https://doi.org/10.1016/j.triboint.2007.01.007.

Bureau, L., Coupier, G., Salez, T., 2023. Lift at low Reynolds number. Eur. Phys. J. E 46, 111. https://doi.org/10.1140/epje/s10189-023-00369-5.

Camacho, G.T., Ortiz, M., 1996. Computational modelling of impact damage in brittle materials. Int. J. Solids Struct. 33, 2899–2938. https://doi.org/10.1016/0020-7683(95)00255-3.

Cameron, A., 1971. Basic Lubrication Theory. Longman.

Carrier, G.F., Pearson, C.E., 2014. Partial Differential Equations: Theory and Technique. Academic Press.

de Vicente, J., Stokes, J.R., Spikes, H.A., 2005. The frictional properties of newtonian fluids in rolling-sliding soft-EHL contact. Tribol. Lett. 20, 273–286. https://doi.org/10.1007/s11249-005-9067-3.

Dong, H., Moyle, N., Wu, H., Khripin, C.Y., Hui, C.-Y., Jagota, A., 2023. The transition from elasto-hydrodynamic to mixed regimes in lubricated friction of soft solid surfaces. Adv. Mater. 35, 2211044 https://doi.org/10.1002/adma.202211044.

Dowson, D., Higginson, G.R., 2014. Elasto-Hydrodynamic Lubrication: International Series on Materials Science and Technology. Elsevier

Essink, M.H., Pandey, A., Karpitschka, S., Venner, C.H., Snoeijer, J.H., 2021. Regimes of soft lubrication. J. Fluid Mech. 915, A49. https://doi.org/10.1017/ifm.2021.96.

Gervais, T., El-Ali, J., Günther, A., Jensen, K.F., 2006. Flow-induced deformation of shallow microfluidic channels. Lab Chip 6, 500–507. https://doi.org/10.1039/

Glover, J.D., Yang, X., Long, R., Pham, J.T., 2023. Creasing in microscale, soft static friction. Nat. Commun. 14, 2362. https://doi.org/10.1038/s41467-023-38091-7. Hong, W., Zhao, X., Suo, Z., 2009. Formation of creases on the surfaces of elastomers and gels. Appl. Phys. Lett. 95, 111901 https://doi.org/10.1063/1.3211917. Hou, J.S., Mow, V.C., Lai, W.M., Holmes, M.H., 1992. An analysis of the squeeze-film lubrication mechanism for articular cartilage. J. Biomech. 25, 247–259. https://doi.org/10.1016/0021-9290(92)90024-U.

Huber, G., Mantz, H., Spolenak, R., Mecke, K., Jacobs, K., Gorb, S.N., Arzt, E., 2005. Evidence for capillarity contributions to gecko adhesion from single spatula nanomechanical measurements. Proc. Natl. Acad. Sci. 102, 16293–16296. https://doi.org/10.1073/pnas.0506328102.

Hui, C.-Y., Wu, H., Jagota, A., Khripin, C., 2021. Friction force during lubricated steady sliding of a rigid cylinder on a viscoelastic substrate. Tribol. Lett. 69, 30. https://doi.org/10.1007/s11249-020-01396-5.

Jahn, S., Seror, J., Klein, J., 2016. Lubrication of articular cartilage. Annu. Rev. Biomed. Eng. 18, 235–258. https://doi.org/10.1146/annurev-bioeng-081514-123305. Jha, A., Amarouchene, Y., Salez, T., 2023. Capillary-lubrication force exerted on a two-dimensional particle moving towards a thin fluid film. J. Fluid Mech. 977, A50. https://doi.org/10.1017/jfm.2023.1016.

Karan, P., Chakraborty, J., Chakraborty, S., 2021. Generalization of elastohydrodynamic interactions between a rigid sphere and a nearby soft wall. J. Fluid Mech. 923, A32. https://doi.org/10.1017/jfm.2021.595.

Karan, P., Chakraborty, J., Chakraborty, S., 2020. Influence of non-hydrodynamic forces on the elastic response of an ultra-thin soft coating under fluid-mediated dynamic loading. Phys. Fluids 32, 022002. https://doi.org/10.1063/1.5134149.

Kaveh, F., Ally, J., Kappl, M., Butt, H.-J., 2014. Hydrodynamic force between a sphere and a soft, elastic surface. Langmuir 30, 11619–11624. https://doi.org/

Lee, C., Shi, H., Jung, J., Zheng, B., Wang, K., Tutika, R., Long, R., Lee, B.P., Gu, G.X., Bartlett, M.D., 2023. Bioinspired materials for underwater adhesion with pathways to switchability. Cell Rep. Phys. Sci. 4, 101597 https://doi.org/10.1016/j.xcrp.2023.101597.

Leroy, S., Steinberger, A., Cottin-Bizonne, C., Restagno, F., Léger, L., Charlaix, É., 2012. Hydrodynamic interaction between a spherical particle and an elastic surface: a gentle probe for soft thin films. Phys. Rev. Lett. 108, 264501 https://doi.org/10.1103/PhysRevLett.108.264501.

- Liu, Z., Dong, H., Jagota, A., Hui, C.-Y., 2022. Lubricated soft normal elastic contact of a sphere: a new numerical method and experiment. Soft Matter 18, 1219–1227. https://doi.org/10.1039/D1SM01654G.
- Ma, S., Scaraggi, M., Wang, D., Wang, X., Liang, Y., Liu, W., Dini, D., Zhou, F., 2015. Nanoporous substrate-infiltrated hydrogels: a bioinspired regenerable surface for high load bearing and tunable friction. Adv. Funct. Mater. 25, 7366–7374. https://doi.org/10.1002/adfm.201503681.
- Martin, A., Clain, J., Buguin, A., Brochard-Wyart, F., 2002. Wetting transitions at soft, sliding interfaces. Phys. Rev. E 65, 031605. https://doi.org/10.1103/PhysRevE.65.031605.
- Maugis, D., 1992. Adhesion of spheres: the JKR-DMT transition using a dugdale model. J. Colloid Interface Sci. 150, 243–269. https://doi.org/10.1016/0021-9797
- Moyle, N., Dong, H., Wu, H., Khripin, C.Y., Hui, C.-Y., Jagota, A., 2021. Increased Sliding Friction of a Lubricated Soft Solid Using an Embedded Structure. Tribol. Lett. 70, 2. https://doi.org/10.1007/s11249-021-01540-9.
- Myant, C., Spikes, H.A., Stokes, J.R., 2010. Influence of load and elastic properties on the rolling and sliding friction of lubricated compliant contacts. Tribol. Int. 43, 55–63. https://doi.org/10.1016/j.triboint.2009.04.034.
- Persson, B.N.J., 2007. Wet adhesion with application to tree frog adhesive toe pads and tires. J. Phys. Condens. Matter 19, 376110. https://doi.org/10.1088/0953-8984/19/37/376110.
- Persson, B.N.J., 2001. Theory of rubber friction and contact mechanics. J. Chem. Phys. 115, 3840-3861. https://doi.org/10.1063/1.1388626.
- Persson, B.N.J., Scaraggi, M., 2009. On the transition from boundary lubrication to hydrodynamic lubrication in soft contacts. J. Phys. Condens. Matter 21, 185002. https://doi.org/10.1088/0953-8984/21/18/185002.
- Persson, B.N.J., Tartaglino, U., Albohr, O., Tosatti, E., 2005. Rubber friction on wet and dry road surfaces: the sealing effect. Phys. Rev. B 71, 035428. https://doi.org/10.1103/PhysRevB.71.035428.
- Reynolds, O., 1997. IV. On the theory of lubrication and its application to Mr. Beauchamp tower's experiments, including an experimental determination of the viscosity of olive oil. Philos. Trans. R. Soc. London 177, 157–234. https://doi.org/10.1098/rstl.1886.0005.
- Roberts, A.D., 1971. Squeeze films between rubber and glass. J. Phys. D Appl. Phys. 4, 423-432. https://doi.org/10.1088/0022-3727/4/3/311.
- Sadowski, P., Stupkiewicz, S., 2019. Friction in lubricated soft-on-hard, hard-on-soft and soft-on-soft sliding contacts. Tribol. Int. 129, 246–256. https://doi.org/10.1016/j.triboint.2018.08.025.
- Saintyves, B., Jules, T., Salez, T., Mahadevan, L., 2016. Self-sustained lift and low friction via soft lubrication. Proc. Natl. Acad. Sci. https://doi.org/10.1073/
- Skotheim, J.M., Mahadevan, L., 2004. Soft lubrication. Phys. Rev. Lett. 92, 245509 https://doi.org/10.1103/PhysRevLett.92.245509.
- Snoeijer, J.H., Eggers, J., Venner, C.H., 2013. Similarity theory of lubricated Hertzian contacts. Phys. Fluids 25, 101705. https://doi.org/10.1063/1.4826981.
- Song, J., Jiang, H., Choi, W.M., Khang, D.Y., Huang, Y., Rogers, J.A., 2008. An analytical study of two-dimensional buckling of thin films on compliant substrates. J. Appl. Phys. 103, 014303 https://doi.org/10.1063/1.2828050.
- Spikes, H.A., 1997. Mixed lubrication an overview. Lubr. Sci. 9, 221-253. https://doi.org/10.1002/ls.3010090302.
- Strobel, C.M., Menezes, P.L., Lovell, M.R., Beschorner, K.E., 2012. Analysis of the contribution of adhesion and hysteresis to shoe-floor lubricated friction in the boundary lubrication regime. Tribol. Lett. 47, 341–347. https://doi.org/10.1007/s11249-012-9989-5.
- Sun, M., Kumar, N., Dhinojwala, A., King, H., 2021. Attractive forces slow contact formation between deformable bodies underwater. Proc. Natl. Acad. Sci. https://doi.org/10.1073/pnas.2104975118.
- Ta, T.D., Tieu, A.K., Zhu, H., Zhu, Q., Kosasih, P.B., Zhang, J., Deng, G., 2016. Tribological behavior of aqueous copolymer lubricant in mixed lubrication regime. ACS Appl. Mater. Interfaces 8, 5641–5652. https://doi.org/10.1021/acsami.5b10905.
- van Limbeek, M.A.J., Essink, M.H., Pandey, A., Snoeijer, J.H., Karpitschka, S., 2021. Pinning-induced folding-unfolding asymmetry in adhesive creases. Phys. Rev. Lett. 127, 028001 https://doi.org/10.1103/PhysRevLett.127.028001.
- Wang, Y., Dhong, C., Frechette, J., 2015. Out-of-contact elastohydrodynamic deformation due to lubrication forces. Phys. Rev. Lett. 115, 248302 https://doi.org/10.1103/PhysRevLett.115.248302.
- Wang, Y., Tan, M.R., Frechette, J., 2017. Elastic deformation of soft coatings due to lubrication forces. Soft Matter 13, 6718–6729. https://doi.org/10.1039/C7SM01061C.
- Wu, H., Hui, C.-Y., Jagota, A., 2023. Solving transient problems in soft Elasto-Hydrodynamic lubrication. J. Mech. Phys. Solids 170, 105104. https://doi.org/10.1016/j.jmps.2022.105104.
- Wu, H., Jagota, A., Hui, C.-Y., 2021. Lubricated sliding of a rigid cylinder on a viscoelastic half space. Tribol. Lett. 70, 1. https://doi.org/10.1007/s11249-021-01537-4.
- Wu, H., Moyle, N., Jagota, A., Hui, C.-Y., 2020. Lubricated steady sliding of a rigid sphere on a soft elastic substrate: hydrodynamic friction in the Hertz limit. Soft Matter 16, 2760–2773. https://doi.org/10.1039/C9SM02447F.
- Zhang, H., Zhang, X., 2020. Solving the Riesz–Feller space-fractional backward diffusion problem by a generalized Tikhonov method. Adv. Differ. Eqs. 2020, 390. https://doi.org/10.1186/s13662-020-02719-5.